Study on the Properties of Nano-TiO_2/Polybutylene Succinate Composites Prepared by Vane Extruder

Jintao Huang, Xiang Lu, Ning Zhang, Li Yang, Ming Yan, Huanyu Liu, Guizhen Zhang, Jinping Qu
National Engineering Research Center of Novel Equipment for Polymer Processing, The Key Laboratory of Polymer Processing Engineering of the Ministry of Education, South China University of Technology, Guangdong, Guangzhou 510640, People's Republic of China

Different proportions of nanoscale TiO_2 (nano-TiO_2)-filled polybutylene succinate (PBS) composites were prepared by vane extruder. The crystalline, thermal, dynamic viscoelastic, mechanical, and UV-resistance properties of the composites were studied, and X-ray diffraction, differential scanning calorimetry, and thermogravimetric analysis were conducted. Results show that the crystalline structure of the PBS composites did not change with TiO_2 addition. TiO_2 almost has no effect on the crystallization and melting behavior of PBS. Nevertheless, the introduction of TiO_2 has improved the thermal stability, tensile modulus, flexural modulus, and flexural strength of the PBS composites. The UV resistance of the composites has also been significantly enhanced with TiO_2 addition. POLYM. COMPOS., 35:53–59, 2014.
© 2013 Society of Plastics Engineers

INTRODUCTION

With the growing concern on energy crisis and environmental protection, biocompatible and biodegradable polymers have attracted significant attention both from ecological and biomedical perspectives in the past decades [1]. Biodegradable aliphatic polyesters such as polybutylene succinate (PBS), polycaprolactone, and polylactic acid have biodegradation properties, biocompatibility, high mechanical strength, and excellent shaping properties. These biodegradable aliphatic polyesters are mainly produced or synthesized from renewable agricultural resources, such as whey, soybean, and corn [2,3]. Therefore, biodegradable polymers have a vast number of potential applications.

PBS is a biodegradable thermoplastic polymer that is produced by the polycondensation reaction between 1,4-butanediol and succinic acid [3]. Unlike other conventional thermoplastic polymers, such as polypropylene and polyethylene, PBS is expensive and has poor mechanical properties. These drawbacks of PBS limit its engineering applications [4]. Reinforcement by inorganic fibers or whiskers has been considered an effective method to improve the properties of polymers and to cheapen the compound [5].

Given its high catalytic performance, excellent stability, non-toxicity, and low material cost, titanium dioxide is often used as catalyst/photocatalyst in water and wastewater treatment [6,7]. The strong oxidation power and super hydrophilic properties of TiO_2 make it an appropriate self-cleaning coating for outdoor purposes [8,9]. Compared with general TiO_2, nanoscale TiO_2 (nano-TiO_2) not only can absorb UV rays but also can scatter UV, thereby enabling nano-TiO_2 take advantage of PBS modification. Research on TiO_2/PBS will help improve the UV performance of TiO_2/PBS. Further research on the composite may also help in the identification of several new surface properties of TiO_2/PBS and in the enhancements of the mechanical properties of TiO_2/PBS. However, few studies on TiO_2/PBS blending have been reported [10].

In this study, different proportions of TiO_2-filled PBS composites were prepared by vane extruder. Polymer vane extruder, which was designed by Prof. J.P. Qu in South China University of Technology, is a novel equipment for polymer processing [11]. The plasticizing and conveying mechanism of the vane extruder is dominated by elongational flow, which is good for the dispersive and distributed mixing of composites. Furthermore, the thermal-mechanical history of the vane extruder is short, leading to the reduction in the degradation of polymer molecules [12–14]. Scanning electron microscopy (SEM), transmission electron microscopy (TEM), X-ray diffraction (XRD), differential scanning calorimetry (DSC), thermogravimetric analysis (TGA), dynamic mechanical properties analysis

Correspondence to: Jinping Qu; e-mail: jpqu@scut.edu.cn
Contract grant sponsor: National Nature Science Foundation of China; contract grant numbers: 10872071, 50973035, 50903033; contract grant sponsor: Fundamental Research Funds for the Central Universities; contract grant number: NO.2011ZM0063; contract grant sponsor: National Key Technology R&D Program of China; contract grant numbers: 2009BAI84B05, 2009BAI84B06; contract grant sponsor: Program for Changjiang Scholars, and Innovative Research Team in University; contract grant number: IRT0827; contract grant sponsor: National Natural Science Foundation of China-Guangdong Joint Foundation Project; contract grant number: U1201242.
DOI 10.1002/pc.22633
Published online in Wiley Online Library (wileyonlinelibrary.com).
© 2013 Society of Plastics Engineers

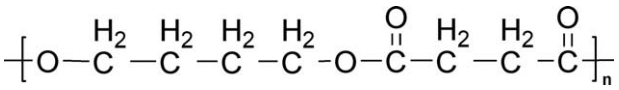

FIG. 1. Chemical structure of PBS.

(DMA), and UV transmittance were used to investigate the effect of TiO_2 on the UV performance and morphological, crystal, thermal, dynamic viscoelastic, and mechanical properties of TiO_2/PBS blends.

EXPERIMENTAL

Materials

PBS (Bionolle 1020MD) was supplied by Showa Highpolymer, Japan. The melt flow index used in this study was 25 g/10 min (190°C, 2.16 kg), and the density was 1.26×10^3 kg m^{-3}. The chemical structure for PBS is presented in Fig. 1.

Nano-TiO_2 (VK-TAKH570, Xuan Cheng Jing Rui New Material, China) with particle size of 20 nm was used in this research.

Extrusion Device

The vane extruder is a type of novel polymer processing equipment that is completely different from traditional screw extruder in terms of structure. As shown in Fig. 2, the vane extruder is composed of a number of vane plasticizing and conveying units (VPCU). The stator, vane, baffle, and rotor of the equipment comprise the closed chamber. Given that the stator has an eccentric distance to the rotor, the volume of the closed chamber surrounded by two baffles periodically changes with rotor rotation during processing. A converging channel can be obtained in the circumferential direction, thus generating a dynamic elongated deformation field. The VPCU feeds materials when the volume of the closed chamber increases, but discharge materials when the volume of the closed chamber decreases [15–18]. Table 1 shows the main parameters of the vane extruder used in this study.

Composite Preparation

PBS and TiO_2 were dried in a vacuum at 60°C for more than 6 h before blending to remove moisture. To obtain a composite material with high powder dispersity, PBS, and TiO_2 was blended and then added to the vane extruder. The blended material was then prepared with PBS containing 10% TiO_2 polymer masterbatch as basic material. Second melt blending was conducted in the vane extruder on the basis of the desired ratio of the basic material and pure PBS. PBS was blended with TiO_2 (0, 0.5, 1, 2, 5, and 10 wt%) by using the vane extruder. The profile temperatures were 110, 115, 120, and 125°C, and the vane speed was 60 rpm. Extruded strands were quenched, pelletized, and dried at 60°C for 24 h. The extruded pellets were compression molded in a hydraulic press at 150°C. The size of tensile test samples: $140 \times 10 \times 4$ mm^3, the size of flexural test samples: $80 \times 10 \times 4$ mm^3, the size of impact test samples: $60 \times 8 \times 4$ mm^3 (the size of gap is 2 mm).

SEM

The fracture surface was studied via SEM (HITACHI S-3700N, Japan). The specimens (4-mm thick) were submerged in liquid nitrogen for ~15 min and fractured to expose the internal structure for SEM investigations. Prior to the SEM test, all surfaces were sputtered with gold to provide enhanced conductivity.

TEM

Transmission electron microscopy observations were carried out using a FEI Tecnai F20 at an acceleration voltage of 200 kV. Sample films were prepared with a thickness of 80 nm using a Leica EMUC6/FC6 microtome.

XRD

D8 ADVANCE (Bruker, Germany) was used for XRD analysis on pure TiO_2, pure PBS, and TiO_2/PBS composites. Scans were made between Bragg angles ranging from 5° to 60° at a scanning rate of 2° min^{-1}.

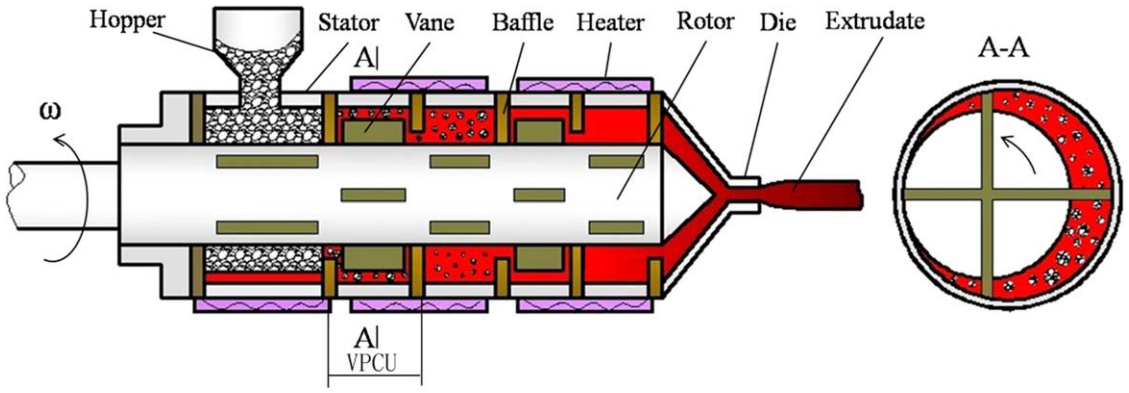

FIG. 2. Schematic diagram of the vane extruder. [Color figure can be viewed in the online issue, which is available at wileyonlinelibrary.com.]

 DOI 10.1002/pc

TABLE 1. Main parameters of the vane extruder.

Number of VPCU	Radius of rotor (r)	Radius of stator (R)	Eccentricity distance (e)	Height of discharging gap (h)	Diameter of rotor (d)	L/d
17	20 mm	23 mm	3 mm	5 mm	40 mm	12

DSC

DSC was performed by using a Netzsch DSC (model 204c, Germany) equipped with liquid nitrogen cooling accessory. Specimens were first heated from room temperature to 150°C, kept for 3 min to eliminate any thermal history, and then cooled to 30°C at 10°C min^{-1} under nitrogen atmosphere. The second scan was performed by reheating the specimens from 30 to 150°C at 10°C min^{-1}. All thermal parameters provided were determined in an average of three repeats.

TGA

TGA of samples (10 mg) was conducted on a thermogravimetic analyzer (Netzsch TG209) at temperatures ranging from 30 to 500°C in air atmosphere (250 mL min^{-1}) with a 10°C min^{-1} heating ramp.

DMA

DMA was performed at temperatures ranging from −120 to 80°C under liquid nitrogen atmosphere by using a Netzsch DMA (model 242c, Germany). The samples had 10 mm × 4 mm × 1 mm dimensions. Tests were performed in a single cantilever bending mode at a fixed frequency of 1 Hz and a heating rate of 3°C min^{-1}.

Mechanical Test

Tensile and flexural test of pure PBS and TiO_2/PBS blends were conducted by using an INSTRON universal machine (model 5566, United States) in accordance with GBT 1447–2005. INSTRON POE2000 pendulum impact tester was used in the impact test in accordance with GBT 1843. All values were determined in an average of five repeats.

UV Transmittance

UV transmittance spectra for composites were obtained by using a UV spectrophotometer (American Elmer Lambda950). The spectra were recorded at room temperature in air in wavelengths ranging from 250 to 450 nm.

RESULTS AND DISSCUSSION

Morphological Investigation

The dispersion state of TiO_2 in the PBS matrix was characterized by SEM and TEM. The SEM images of the fracture surface for the pure PBS and TiO_2/PBS blends with different TiO_2 loadings are shown in Fig. 3. And the morphology of 10 wt% TiO_2/PBS was also investigated by TEM (Fig. 4). The dark areas represent the TiO_2 inorganic phase. Through SEM and TEM test method, it can be found that no obvious reunion phenomenon was observed on the picture, thus illustrating that nano-TiO_2 could be distributed homogeneously in the PBS polymer matrix [19,20].

Crystalline Structure

The crystalline structures of TiO_2, pure PBS, and TiO_2/PBS composites investigated by XRD are shown in Fig. 5. Pure TiO_2 shows the following five reflection peaks around 2θ: 27.5°, 37.0°, 41.3°, 54.4°, and 56.7°. Pure PBS exhibits three sharp reflection peaks at 2θ, namely, 19.6°, 22.7°, and 29.2°. These peaks indicate the formation of monoclinic crystals and the diffraction of the (020), (110), and (111) planes, respectively [21]. The TiO_2/PBS composites also had similar reflection peaks with those of pure PBS, thus denoting that the crystalline structure of PBS was not changed by the addition of TiO_2. The intensity of these peaks also decreased with increased TiO_2 content [22,23].

Thermal Properties

The DSC nonisothermal curves of pure PBS and TiO_2/PBS blends at cooling rate of 10°C min^{-1} are shown in Fig. 6a. Table 2 shows the crystallization temperature (T_c), melting enthalpy (ΔH_m), and percent crystallinity (X_c) of pure PBS and TiO_2/PBS blends. The X_c of pure PBS and TiO_2/PBS blends were determined by *Eqs.* 1 and 2, respectively [24]. The melting enthalpy of 100% crystalline PBS (ΔH_m^0) is 110.3 J g^{-1} and W_f is the weight fraction of TiO_2 in the composite [25].

$$X_c = \frac{\Delta H_m}{\Delta H_m^o} \times 100\% \quad (1)$$

$$X_c = \frac{\Delta H_m}{\Delta H_m^o (1 - W_f)} \times 100\% \quad (2)$$

Table 2 shows the crystallization exotherms of pure PBS and of TiO_2/PBS blends. The crystallization peak temperatures (T_c) at a constant cooling rate of 10°C min^{-1} for all investigated samples are ~77°C. This finding suggests the independence of the samples on TiO_2 content. As shown in Table 2, the degree of crystallinity (X_c) of TiO_2/PBS decreases with increasing TiO_2 content. These phenomena indicate that TiO_2 does not play an active role in the heterogeneous nucleation of polymer resin [26].

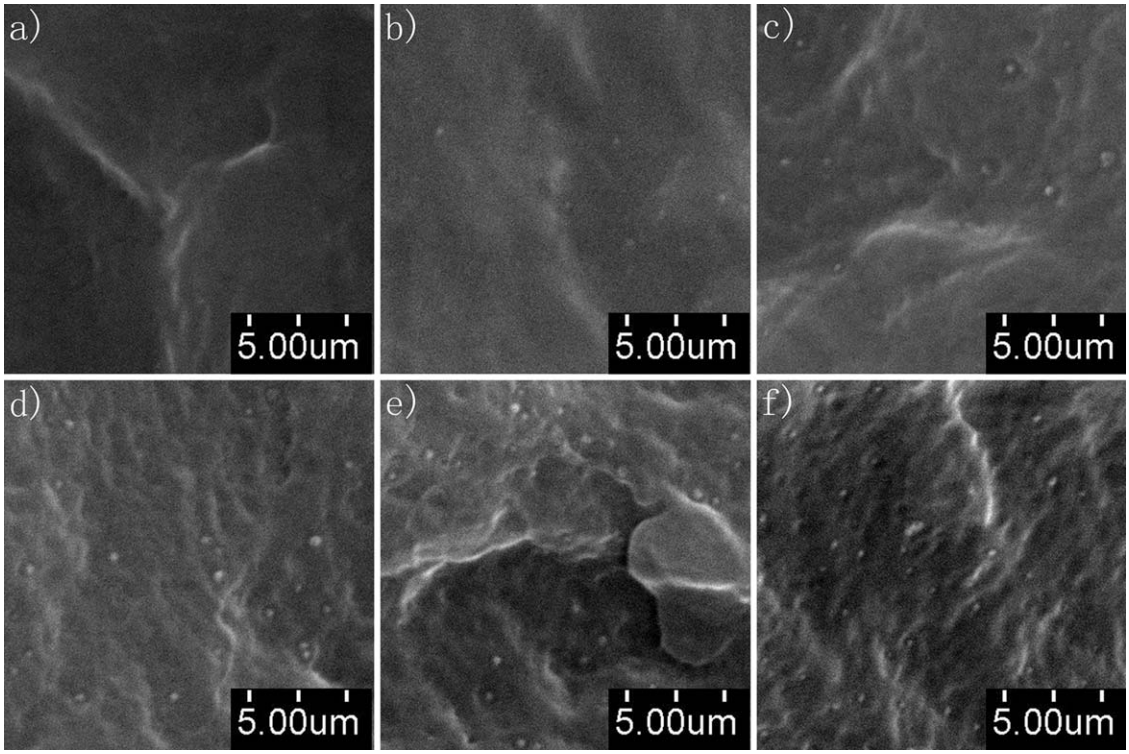

FIG. 3. SEM micrographs of fracture surfaces for (a) pure PBS, (b) 0.5 wt% TiO_2/PBS, (c) 1 wt% TiO_2/PBS, (d) 2 wt% TiO_2/PBS, (e) 5 wt% TiO_2/PBS, and (f) 10 wt% TiO_2/PBS.

The melting behavior of pure PBS and blends were also investigated by DSC. Figure 6b shows the heating curves at a heating rate of 10°C min^{-1}. The values of the melting peak temperature (T_m) are almost stable (about 114°C), as shown in Table 2. Thus, TiO_2 almost has no effect on the melting process of PBS [27].

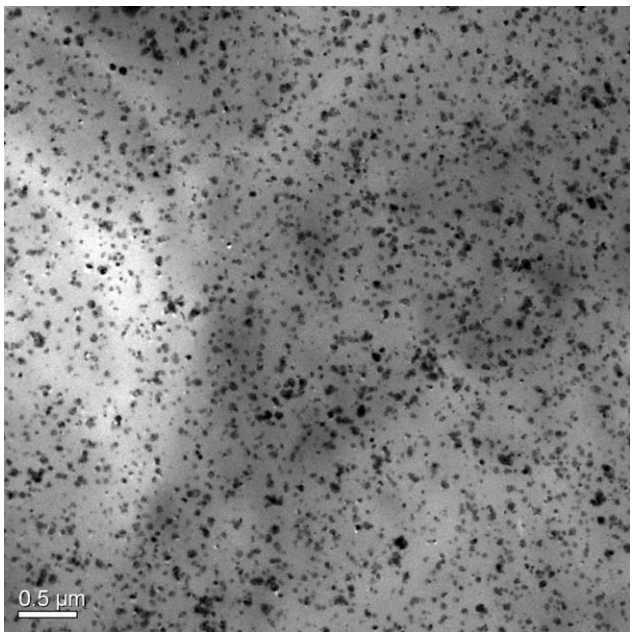

FIG. 4. TEM micrograph of 10 wt% TiO_2/PBS.

Figure 7 and Table 3 show the thermal stability of pure PBS and TiO_2/PBS blends. The onset degradation (defined by the temperature at 5 wt% loss, $T_{0.05}$) as well as the char formation at 500°C were reported in Table 3. As expected, the char formation at 500°C is higher for blends with the TiO_2 than that of pure PBS. The reason is that there was only inorganics left in the system around 500°C. The onset degradation temperature ($T_{0.05}$) for pure PBS, 5 wt% TiO_2/PBS and 10 wt% TiO_2/PBS were

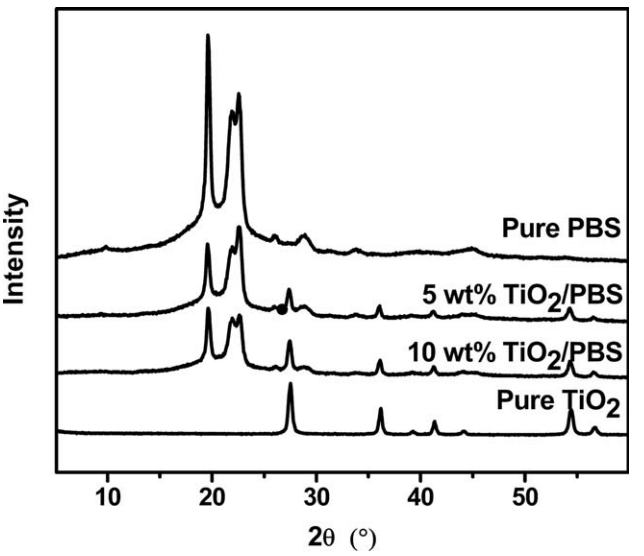

FIG. 5. XRD patterns of TiO_2, pure PBS, and TiO_2/PBS composites.

DOI 10.1002/pc

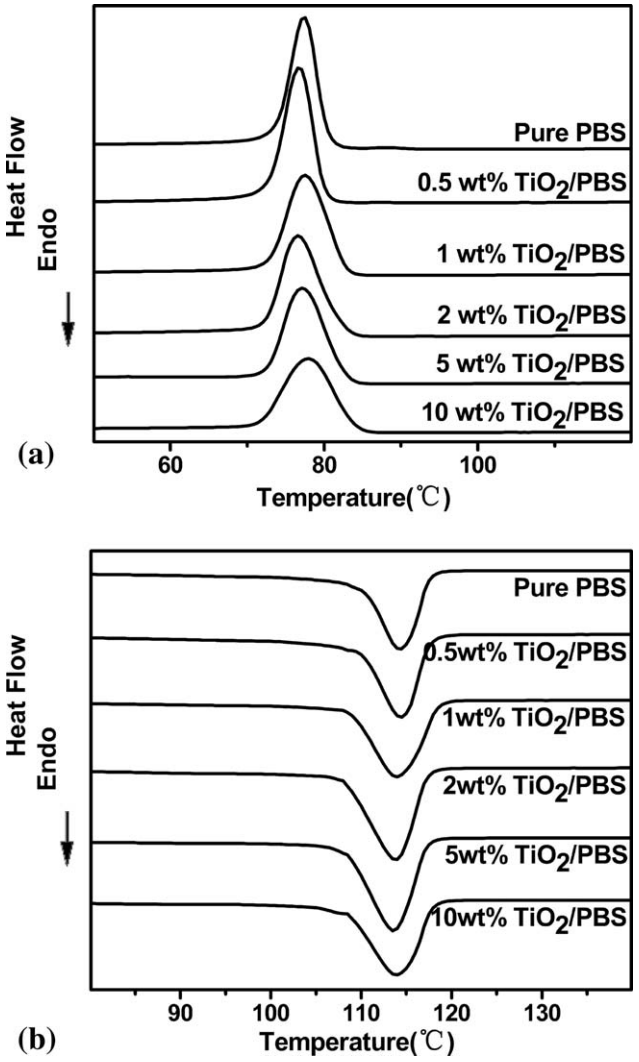

FIG. 6. (a) DSC non-isothermal crystallization curves and (b) DSC melting curves of pure PBS and TiO_2/PBS blends.

335.9, 341.1, 347.3°C, respectively. It was found that the blends have increased the onset degradation temperature and the introduction of inorganic TiO_2 into organic materials tends to improve their thermal stability. This is because the TiO_2 act as heat barrier in the early stages of thermal decomposition [28,29].

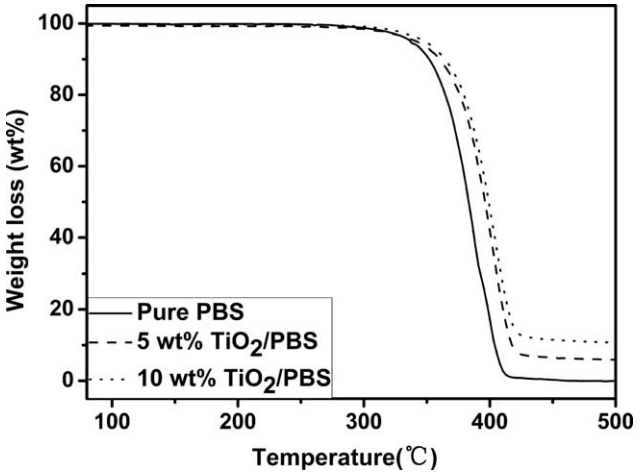

FIG. 7. TGA of pure PBS, 5 wt% TiO_2/PBS, and 10 wt% TiO_2/PBS.

TABLE 2. Crystallization temperature (T_c), melting enthalpy (ΔH_m), percent crystallinity (X_c), and melting temperature (T_m) of pure PBS and TiO_2/PBS blends.

Samples	T_c (°C)	ΔH_m (J g^{-1})	X_c (%)	T_m (°C)
Pure PBS	77.3	62.92	57.04	114.4
0.5 wt% TiO_2/PBS	76.4	61.80	56.03	114.5
1 wt% TiO_2/PBS	77.4	58.52	53.06	114.0
2 wt% TiO_2/PBS	76.3	58.38	52.93	113.9
5 wt% TiO_2/PBS	76.8	57.10	51.77	113.5
10 wt% TiO_2/PBS	77.8	57.07	51.74	113.9

DMA

Figure 8 illustrates the temperature dependence of storage modulus (E') and tan δ of pure PBS and TiO_2/PBS blends. Figure 8a shows that the enhancements in E' are 4.02% for 5 wt% TiO_2/PBS and 8.20% for 10 wt% TiO_2/PBS in temperatures ranging from −100 to −50°C. The sharp drop in E' was observed in temperatures ranging from −50 to 0°C. This temperature decrease is associated with the glass transition temperature (T_g) of the PBS amorphous phase [30]. In temperatures ranging from 0 to 60°C, the E' of all the samples were almost the same. The presence of TiO_2 in the PBS matrix results in a slight temperature decrease of the tan δ peaks of TiO_2/PBS blends (Fig. 8b). This behavior may be caused by the restricted segmental motions at the inorganic–organic interface neighborhood of intercalated TiO_2/PBS blends [31].

Mechanical Properties

The impact strength for pure PBS and TiO_2/PBS blends with different TiO_2 loadings are summarized in Fig. 9. TiO_2 has little effect on the impact strength of the composite material. Nevertheless, a slight increase of impact strength was observed with increased TiO_2 loading. This increase in impact strength could be attributed to the binding force generated between the interface of the TiO_2 and PBS matrix when the composite material is subjected to impact force and to the several TiO_2 particles pulled out from the PBS matrix that absorb some impact energy [32]. As rigid nanoparticles dispersed well and composites haven't appeared reunion phenomenon, the impact strength of PBS is not influenced obviously by the

TABLE 3. Percentage of char formation for pure PBS and TiO_2/PBS blends at 500°C.

Samples	$T_{0.05}$ (°C)	Char at 500°C (%)
Pure PBS	335.9	0.02
5 wt% TiO_2/PBS	341.1	5.89
10 wt% TiO_2/PBS	347.3	10.70

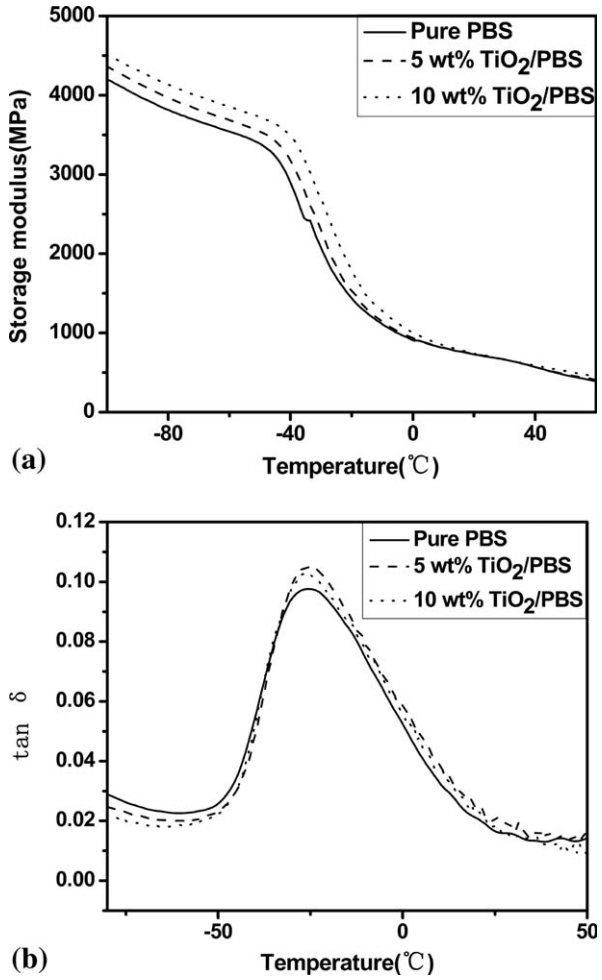

FIG. 8. Temperature dependence of (a) storage modulus (E') and (b) tan δ for pure PBS and various TiO_2/PBS blends.

addition of TiO_2. Therefore the addition of TiO_2 on the impact strength of PBS is kind of small [33].

Figure 10 shows the flexural modulus and flexural strength for pure PBS and TiO_2/PBS blends with different TiO_2 loadings. As shown in Fig. 10, the flexural modulus increased from 467.17 to 636.73 MPa as the TiO_2 loading

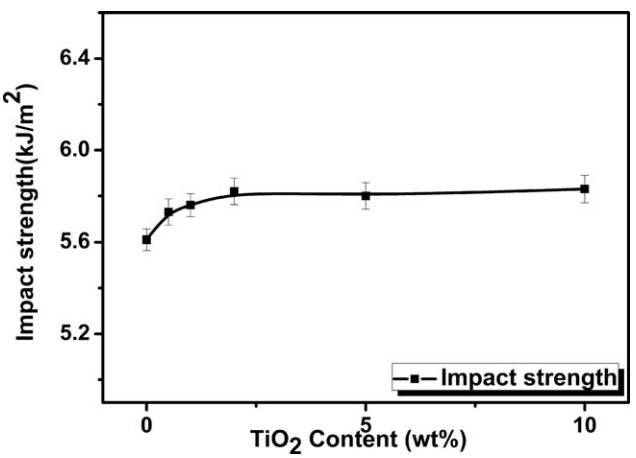

FIG. 9. Impact strength of pure PBS and TiO_2/PBS blends.

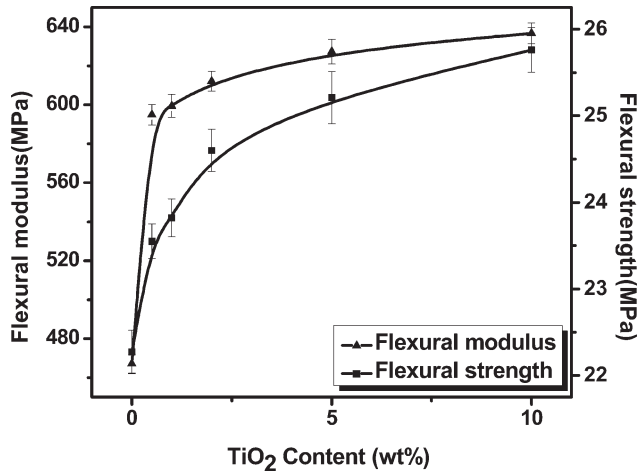

FIG. 10. Flexural modulus and flexural strength of pure PBS and TiO_2/PBS blends.

increased from 0 to 10 wt%. The flexural modulus of composites improved by 36.3% with the 10 wt% TiO_2 addition [2,34]. The flexural strength of pure PBS and TiO_2/PBS blends had similar flexural modulus trends.

The tensile modulus and tensile strength of pure PBS and TiO_2/PBS blends are shown in Fig. 11. The tensile strength of the blends decreased from 31.6 to 25.5 MPa with increased TiO_2 loading and was lower than that of pure PBS (37.2 MPa). Even though TiO_2 has little effect on the tensile strength of the composite material, a slight decrease in tensile strength was observed on the material with the increase in TiO_2 loading. The tensile modulus for pure PBS was 109.43 MPa. The tensile modulus increased slightly and then increased sharply with increasing TiO_2 loading. The tensile modulus of 10 wt% TiO_2/PBS was higher by ~15.5% compared with that of pure PBS.

UV Transmittance

Figure 12 shows the UV absorption spectrum of the composite films that have the same thicknesses but different TiO_2 fractions. Increasing the TiO_2 content improves

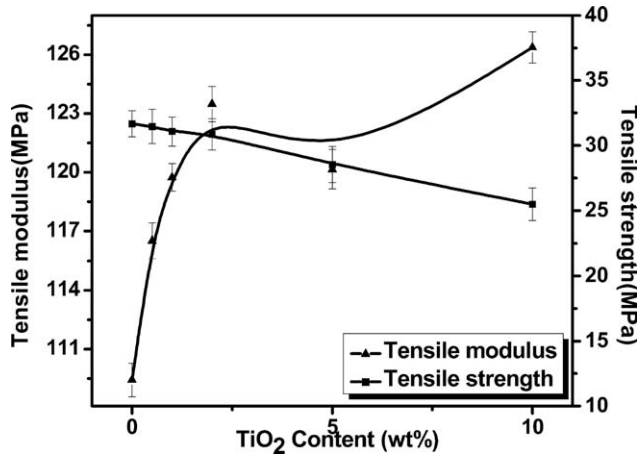

FIG. 11. Tensile modulus and tensile strength of pure PBS and TiO_2/PBS blends.

DOI 10.1002/pc

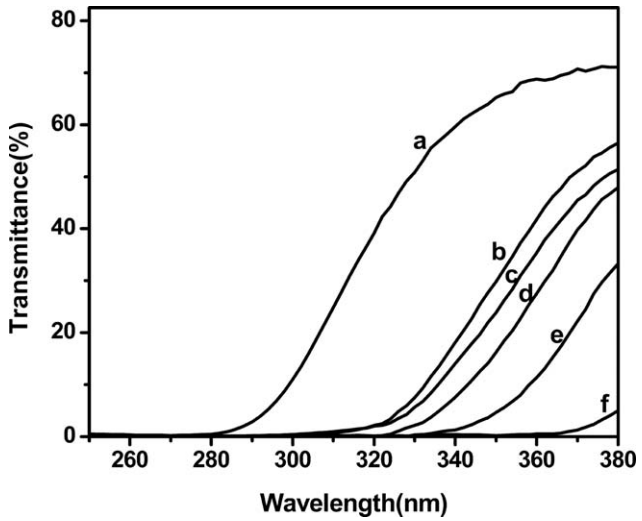

FIG. 12. Transmittance spectra of films on glass substrates for (a) pure PBS, (b) 0.5 wt% TiO_2/PBS, (c) 1 wt% TiO_2/PBS, (d) 2 wt% TiO_2/PBS, (e) 5 wt% TiO_2/PBS, and (f) 10 wt% TiO_2/PBS.

the UV resistance of the system. This improvement is mainly caused by the quantum size effect of TiO_2, which results in electronic energy levels near the Fermi level reach discrete energy levels, thus resulting in band gap increase. Coulomb interaction exists in light-generated electron–hole pairs. Therefore, strong bonds from space make the absorption peaks of the electron–hole pair shift to the shortwave direction [35].

CONCLUSION

This article investigates the effect of TiO_2 content on the properties of TiO_2/PBS composites. Results show that TiO_2 can be uniformly dispersed in the PBS matrix via elongational flow. TiO_2 addition improves the flexural properties of PBS composites. An increase in TiO_2 content results in PBS composites with high thermal degradation content and high storage modulus. However, TiO_2 almost has no effect on the crystallization and melting behavior of PBS, and the crystalline structure of PBS did not change despite the addition of TiO_2. Nevertheless, the incorporation of TiO_2 could improve the UV resistance of pure PBS, thereby providing a new technical method for functional PBS nanocomposite development.

REFERENCES

1. T.M. Wu and C.Y. Wu, *Polym. Degrad. Stab.*, **91**, 2198 (2006).
2. J.Y. Liu, L. Ren, Q. Wei, J.L. Wu, S. Liu, Y.J. Wang, G.Y. Li, *Polym. Compos.*, **33**, 501 (2012).
3. Y.Q. Zhao, J.P. Qu, Y.H. Feng, Z.H. Wu, F.Q. Chen, and H.L. Tang, *Polym. Adv. Technol.*, **23**, 632 (2012).
4. F. Li, H. Yang, Z.Q. Guo, Z.Y. Wang, Y. Wang, D.B. Liu, H.M. Xia, and S. Chen, *J. Northeast Normal Univ. (Nature Sci.)*, **43**, 127 (2011).
5. J.C. Wang, K. Yang, and S.J. Lu, *High Perform Polym.*, **23**, 141 (2011).
6. S. Chin, K. Chiang, and A.G. Fane, *J. Membr. Sci.*, **275**, 202 (2006).
7. Y. Park, W. Kim, H. Park, T. Tachikawa, T. Majima, and W. Choi, *Appl. Catal. B Environ.*, **91**, 355 (2009).
8. A. Nakajima, S. Koitzumi, T. Watanabe, and K. Hashimoto, *Langmuir.*, **16**, 7048 (2000).
9. J. Kasanen, M. Suvanto, and T.T. Pakkanen, *J Appl. Polym. Sci.*, **111**, 2597 (2009).
10. Q.J. Wang, F. Zhu, G.X. Sun, and Q.F. Zhou, *China Leather*, **36**, 9 (2007).
11. J.P. Qu, Z.T. Yang, and X.C. Yin, *Polym. Plast. Technol. Eng.*, **48**, 1269 (2009).
12. J.P. Qu, L.M. Liu, and B. Tan, *Polym. Compos.*, **33**, 185 (2012).
13. J.P. Qu, *CN. Eng. Sci.*, **10**, 20 (2012).
14. J.P. Qu, X.Q. Zhao, J.B. Li, and S.Q. Cai, *J. Appl. Polym. Sci.*, **127**, 3923 (2012).
15. J.P. Qu, H.Z. Chen, S.R. Liu, B. Tan, L.M. Liu, X.C. Yin, Q.J. Liu, and R.B. Guo, *J. Appl. Polym. Sci.*, **128**, 3576 (2012).
16. J.P. Qu, G.Z. Zhang, H.Z. Chen, X.C. Yin, and H.Z He, *Polym. Eng. Sci.*, **52**, 2147 (2012).
17. J.P. Qu, Z.T. Yang, X.C. Yin, H.Z. He, and Y.H. Feng, *Polym. Plast. Technol.*, **48**, 1269 (2009).
18. J.P. Qu, CN Patent, 10026054 2008.1.25. (2008).
19. K.S. Huang, Y.H. Nien, J.S. Chen, T.R. Shieh, and J.W. Chen, *Polym. Compos.*, **27**, 195 (2006).
20. B. Walid, M. Flavien, B.L. Veronique, and C. Philippe, *Mater. Chem. Phys.*, **134**, 399 (2012).
21. B. Tan, J.P. Qu, L.M. Liu, Y.H. Feng, and Y.C. Yin, *Thermochim. Acta*, **525**, 141 (2011).
22. Y. Ichikawa, H. Kondo, Y. Lgarashi, K. Noguchi, K. Okuyama, and J. Washyama, *Polymer*, **41**, 4719 (2000).
23. L. Tan, Y. Chen, W. Zhou, H. Nie, F. Li, and X. He, *Polym. Degrad. Stab.*, 95, 1920 (2010).
24. H.J. Duan, Study Long Chain Branch Reac. *Polypropylene* **23** (2009).
25. Y.J. Phua, W.S. Chow, and Z.A. Mohd Ishak, *Polym. Degrad. Stab.* **96**, 1194 (2011).
26. A. Buzarovska and A. Grozdanov, *J. Appl. Polym. Sci.*, **123**, 2187 (2012).
27. N. Ning, H. Deng, F. Luo, Q. Zhang, K. Wang, F. Chen, and Q. Fu, *Polym. Adv. Technol.*, **23**, 431 (2012).
28. S.S. Ray and M. Okamoto, *Prog. Polym. Sci.*, **28**, 1539 (2003).
29. O. Vincent and C. Hastings, *Macromol. Mater. Eng.*, **296**, 865 (2011).
30. A.J. Uddin, J. Araki, and Y. Gotoh, *Polym. Int.*, **60**, 1230 (2011).
31. X. Wang, H. Yang, L. Song, Y. Hu, W. Xing, and H. Lu, *Compos. Sci. Technol.*, **72**, 1 (2011).
32. J. Zhou, *J. CIESC.*, **61**, 243. (2010).
33. H.R. Peng, *Res. Inorg. Nano-Particles Polym. Compos.*, 52 (2004).
34. C. Rachman, B. Laura, and G.B. David, *J. Am. Ceram. Sac.*, **72**, 1636. (1989).
35. L.D. Zhang and J.M. Mou, *Nano-Mater. Nano-Struct.*, 420 (2001).